Supporting Information

Electronic Structure Modulation of β-$Ni(OH)_2$ Nanocatalyst via La Doping for Boosting Urea Electrooxidation

Quan Zhang,[a] Hejin Ma,[a] Chenyu Zhang,[a] Xin Gao,[a] Cairui Sun,[a] Liangqi Gui,[d] Rufang Zhao,*[a] Fangqi Yang*[c] and Huihui Lin*[b]

[a] Hubei Key Laboratory of Pollutant Analysis and Reuse Technology, College of Chemistry and Chemical Engineering, Hubei Normal University, Huangshi 435002, China

[b] Institute of Sustainability for Chemicals, Energy and Environment ($ISCE^2$), Agency for Science, Technology and Research (A*STAR) Singapore 627833, Singapore

[c] Centre for Molecular Systems and Organic Devices, Key Laboratory for organic Electronics and Information Displays & Jiangsu Key Laboratory for Biosensors, Institute of Advanced Materials (IAM), Nanjing University of Posts and Telecommunications, 9 Wenyuan Road, Nanjing 210023, China.

[d] Jiangxi Key Laboratory of Advanced Ceramic Materials, Energy Storage and Conversion Ceramic Materials Engineering Laboratory of Jiangxi Province, School of Materials Science and Engineering, Jingdezhen Ceramic University, Jingdezhen 333403, China.

Table of Contents

S1. Experimental Section

Chemicals and materials

Nickel chloride hexahydrate ($NiCl_2 \cdot 6H_2O$), ammonium chloride (NH_4Cl) and lanthanum chloride heptahydrate ($LaCl_3 \cdot 7H_2O$) were provided from Macklin Reagent Company. Ltd. Sodium hydroxide (NaOH) was purchased from Sinopharm Chemical Reagent Co. Carbon papers were obtained from Toray Industries, Inc. The reagents used in the experimental process have not been purified. All water used in the experiments was deionized water (18.2 MΩ·cm).

Sample synthesis

Typically, 0.167 g of nickel chloride hexahydrate ($NiCl_2 \cdot 6H_2O$), 0.214 g of ammonium chloride (NH_4Cl), and varying amounts of lanthanum chloride heptahydrate ($LaCl_3 \cdot 7H_2O$) were dissolved in 20 mL of deionized water. Subsequently, 0.055 g of sodium hydroxide (NaOH) was added to the solution, followed by continuous stirring for 20 minutes. The mixture was then sealed in a 40 mL glass vial and placed in a 55 ^oC vacuum oven for 15 hours, producing a green suspension. After cooling to room temperature, the suspension was collected by filtration, washed thoroughly three times with deionized water and ethanol to remove residual reactants and impurities, and finally dried overnight in a vacuum oven at 60 ^oC. The obtained samples were uniformly ground for further use. The corresponding masses of $LaCl_3 \cdot 7H_2O$ used for doping were 0.013 g, 0.026 g, 0.039 g, and 0.052 g, and the resulting catalysts were designated as La-$Ni(OH)_2$-1, La-$Ni(OH)_2$-2, La-$Ni(OH)_2$-3, and La-$Ni(OH)_2$-4, respectively. The sample prepared under identical conditions without the addition of $LaCl_3 \cdot 7H_2O$ was

named $Ni(OH)_2$.

Materials characterization

The material phase was characterized by X-ray powder diffraction (XRD) using a Bruker AXS D8-Focus diffractometer (Germany) with Cu Kα radiation. XRD patterns were recorded in the 2θ range of 10^o–80^o at a scanning rate of 5^o min^{-1}. Surface chemical states were analyzed by X-ray photoelectron spectroscopy (XPS) on a Thermo Scientific K-Alpha spectrometer, with all binding energies calibrated relative to the adventitious C1s peak at 284.8 eV. Morphological features were examined using scanning electron microscopy (SEM, Hitachi SU8010, Japan) under high-vacuum conditions. Prior to imaging, the catalyst samples were sputter-coated with a thin gold layer to improve conductivity. Further microstructural and ultrastructural details were obtained by transmission electron microscopy (TEM) on a JEOL JEM-2010 instrument (Japan) operated at an acceleration voltage of 120 kV.

Electrochemical measurements

All electrochemical measurements were conducted at room temperature using a CHI 660F electrochemical workstation (CH Instruments, China). A standard three-electrode system was employed, consisting of a working electrode (1.0 cm × 1.0 cm carbon paper), a counter electrode (graphite rod), and a reference electrode (Hg/HgO, 1 M KOH). The catalyst ink was prepared by dispersing 5 mg of the catalyst and 1 mg of carbon powder in a mixture of 600 μL ethanol and 10 μL of 5.0 wt% Nafion solution, followed by ultrasonication for 20 minutes. The resulting homogeneous ink was then drop-cast onto the carbon paper substrate (1.0 cm × 1.0 cm) and dried at room

temperature. Electrocatalytic performance was evaluated in an aqueous solution of 1 M KOH with 0.33 M urea. Prior to testing, the working electrode was activated by performing 20 cycles of cyclic voltammetry (CV) between 0.8 and 1.6 V vs. RHE at a scan rate of 50 mV s^{-1} in 1 M KOH. CV curves were then recorded at a scan rate of 10 mV s^{-1} in both 1 M KOH without urea and with 0.33 M urea. To determine the electrochemical double-layer capacitance (C_{dl}), CV scans were performed within a non-Faradaic potential window of 0.8–0.9 V vs. RHE at various scan rates ranging from 10 to 100 mV s^{-1}. Electrochemical impedance spectroscopy (EIS) measurements were carried out at the potential corresponding to a current density of 10 mA cm^{-2}, with a frequency range from 100 kHz to 0.05 Hz. Catalyst stability was assessed through prolonged CV cycling and chronoamperometry tests. The CV stability test was performed at scan rate of 100 mV s^{-1}. All reported potentials were calibrated with respect to the reversible hydrogen electrode (RHE).

Computational methods

The first-principles calculations in this work were conducted using the Vienna Ab initio Simulation Package (VASP 5.4.4)[1, 2]. These simulations were based on density functional theory (DFT), utilizing a plane-wave basis set in conjunction with the projector augmented wave (PAW) method[3, 4]. The exchange-correlation interactions were modeled with the Perdew-Burke-Ernzerhof (PBE) functional under the generalized gradient approximation (GGA)[5]. A plane-wave kinetic energy cutoff of 450 eV was employed to expand the electronic wave functions. The DFT-D3 scheme with Becke–Johnson damping was included to describe the van der Waals interactions[6].

The model of the lanthanum-doped c (La-$Ni(OH)_2$) catalyst was constructed by

substituting a single nickel atom on the surface with a lanthanum atom. A 15 Å vacuum spacing was applied along the surface normal to prevent interactions between adjacent $Ni(OH)_2$ layers. A Monkhorst-Pack *k*-point mesh of 2 × 2 × 1 was used for sampling the Brillouin zone[7]. Atomic positions were optimized via the conjugate gradient method, with convergence thresholds set to 0.03 eV/Å for atomic forces and 1×10^{-5} eV for total energy. The geometry optimization was performed with no constraints on all atoms.

The adsorption energy (ΔE_{ads}) of an adsorbate on the $Ni(OH)_2$ and La-$Ni(OH)_2$ surfaces is given by the expression:

$$\Delta E_{ads} = E_{adsorbate/surface} - E_{surface} - E_{adsorbate}$$

In this expression, $E_{adsorbate/surface}$, $E_{surface}$, and $E_{adsorbate}$ are the total energy of adsorbate and substrate system in the equilibrium state, the energy of pristine surface slab, and the energy of the free adsorbate molecule, respectively. A more negative value of ΔE_{ads} implies enhanced thermodynamic stability for the adsorption configuration.

S2. Structure characterization of catalysts

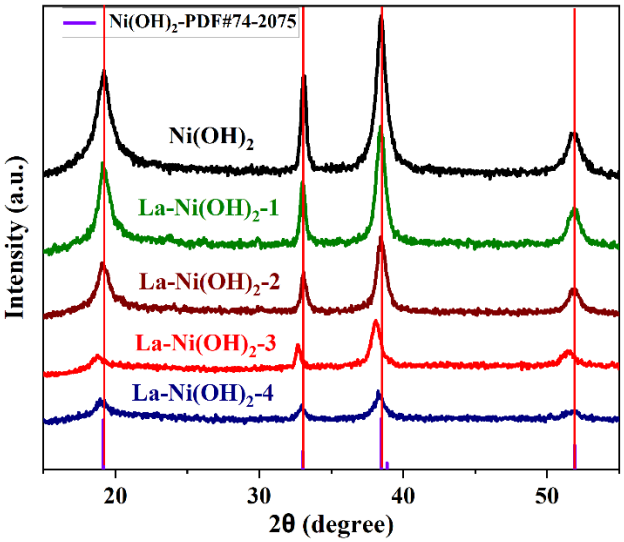

Figure S1. Enlarged XRD patterns of various La-$Ni(OH)_2$ and $Ni(OH)_2$ catalysts.

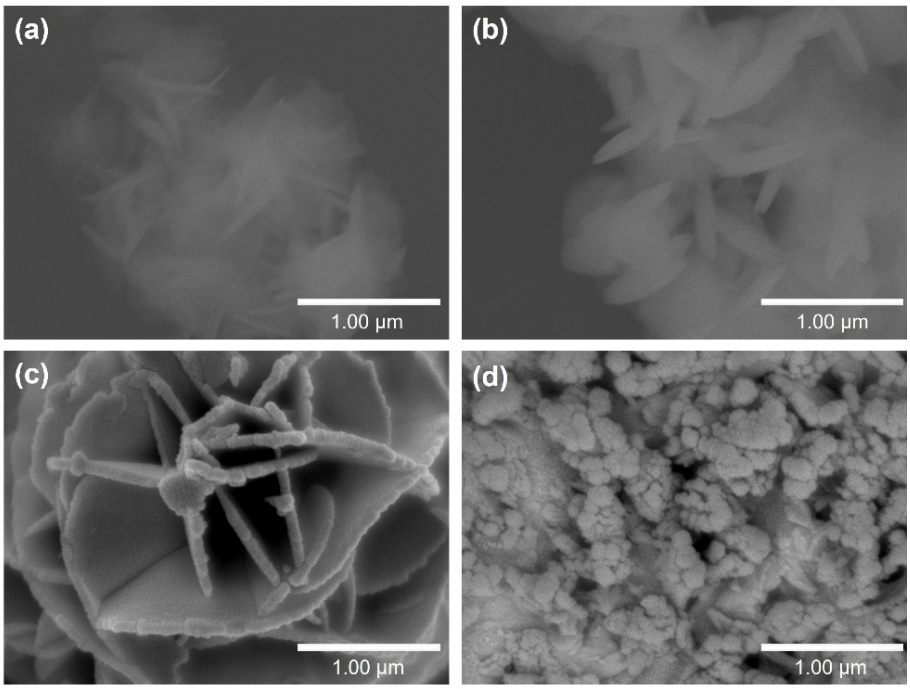

Figure S2. SEM images of (a) $Ni(OH)_2$, (b) La-$Ni(OH)_2$-1, (c) La-$Ni(OH)_2$-2 and (d) La-$Ni(OH)_2$-4 electrocatalysts.

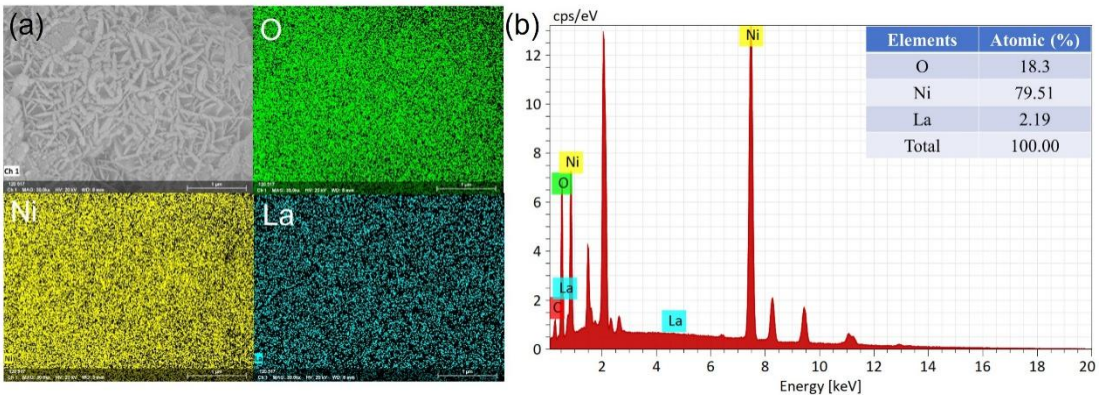

Figure S3. (a) SEM images and corresponding EDX mapping of O, Ni and La for La-$Ni(OH)_2$-3 catalyst. (b) SEM-EDX spectrum and atomic ratios of identified elements for La-$Ni(OH)_2$-3 electrocatalyst.

The SEM-EDS analysis displays the uniform distribution of elements and atomic content ratio of La, Ni, and O in La-$Ni(OH)_2$-3 catalyst.

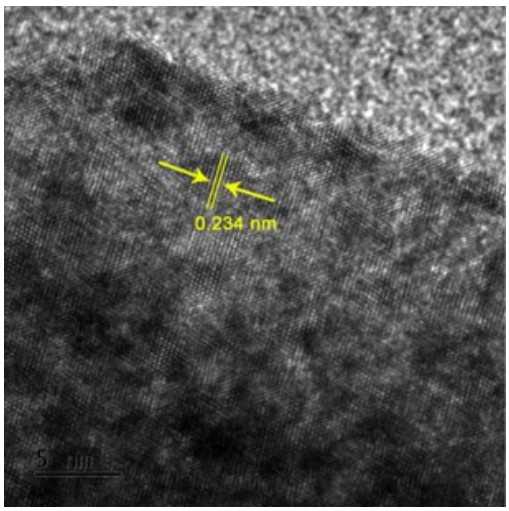

Figure S4. HRTEM of $Ni(OH)_2$ electrocatalyst.

S5. Electron paramagnetic resonance (EPR) test

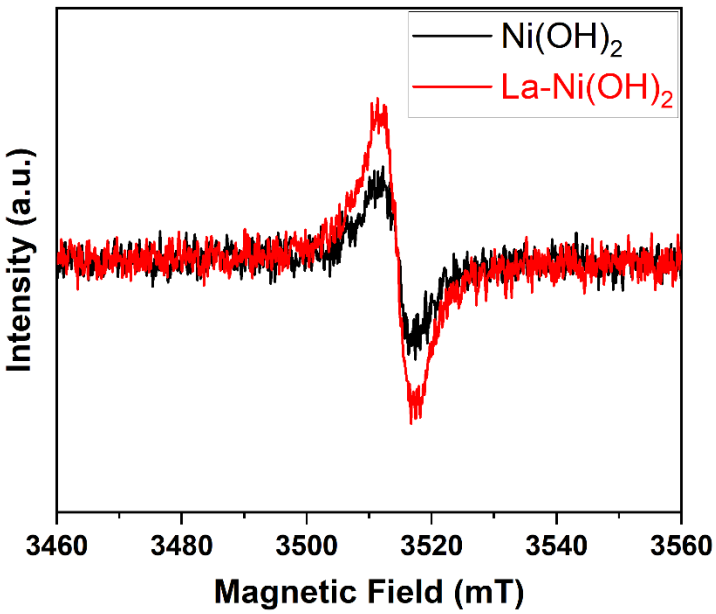

Figure S5. EPR test of $Ni(OH)_2$ and La-$Ni(OH)_2$-3 samples.

S3. UOR tests of catalysts

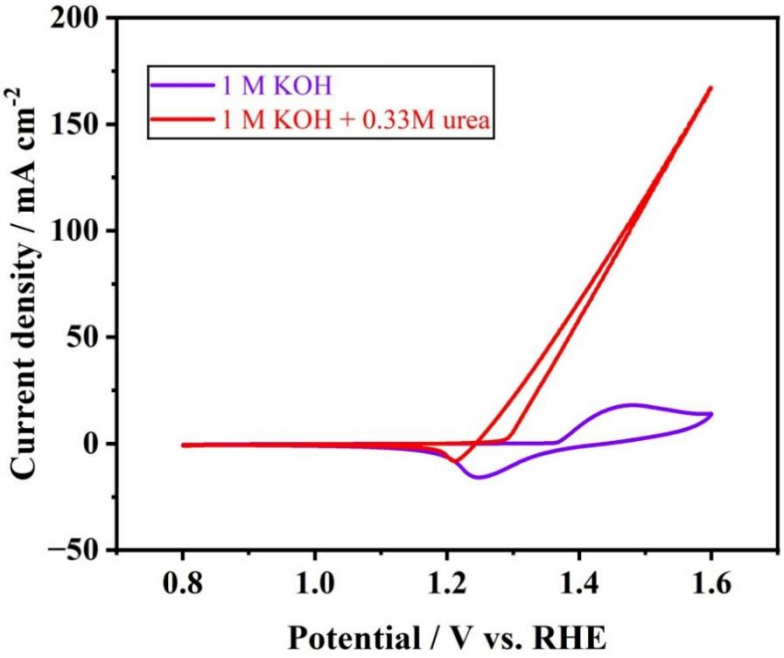

Figure S6. The curves of La-$Ni(OH)_2$-3 catalyst in 1 M KOH with 0.33 M urea solution.

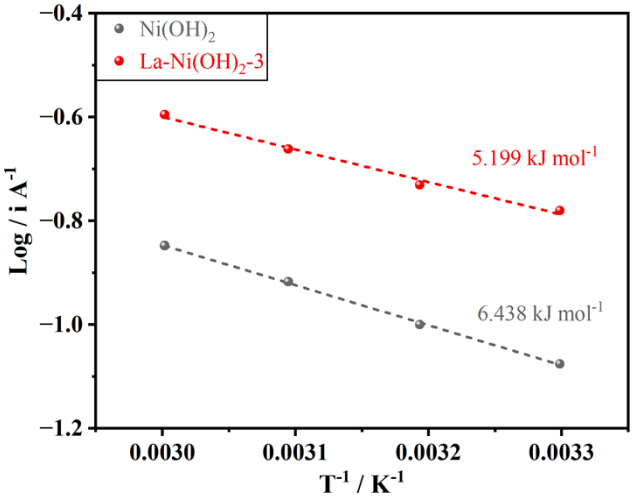

Figure S7. The Arrhenius plots of curves of $Ni(OH)_2$ and La-$Ni(OH)_2$-3 catalysts.

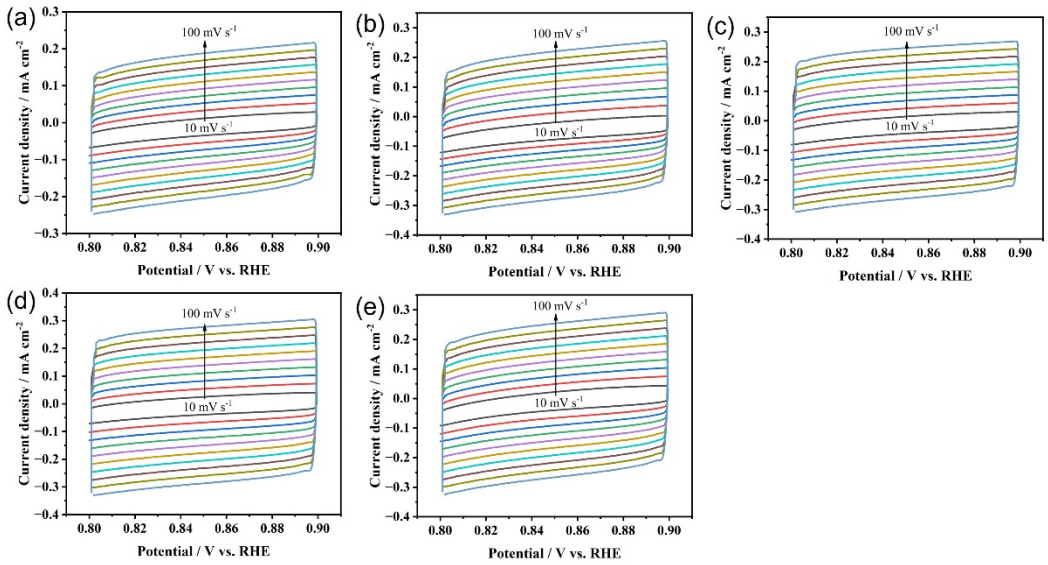

Figure S8. The CV curves in non-Faradaic region of (a) $Ni(OH)_2$, (b) La-$Ni(OH)_2$-1, (c) La-$Ni(OH)_2$-2, (d) La-$Ni(OH)_2$-3 and (e) La-$Ni(OH)_2$-4 electrocatalysts.

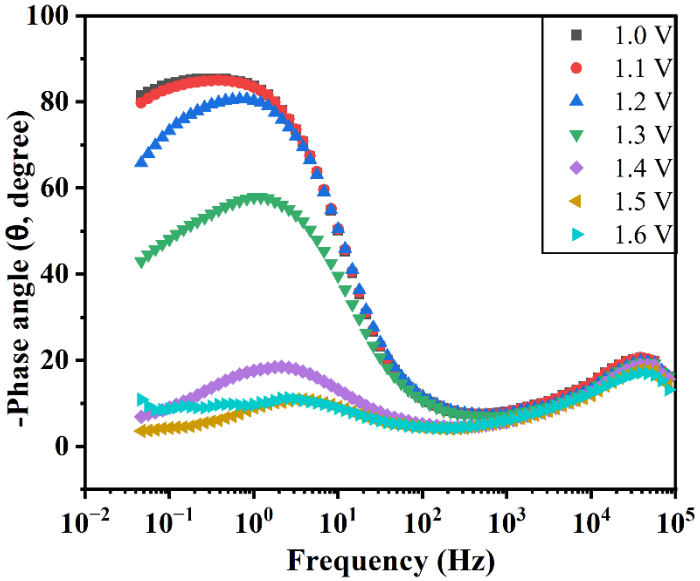

Figure S9. The Bode plots for $Ni(OH)_2$ catalysts in 1 M KOH + 0.33 M urea solution.

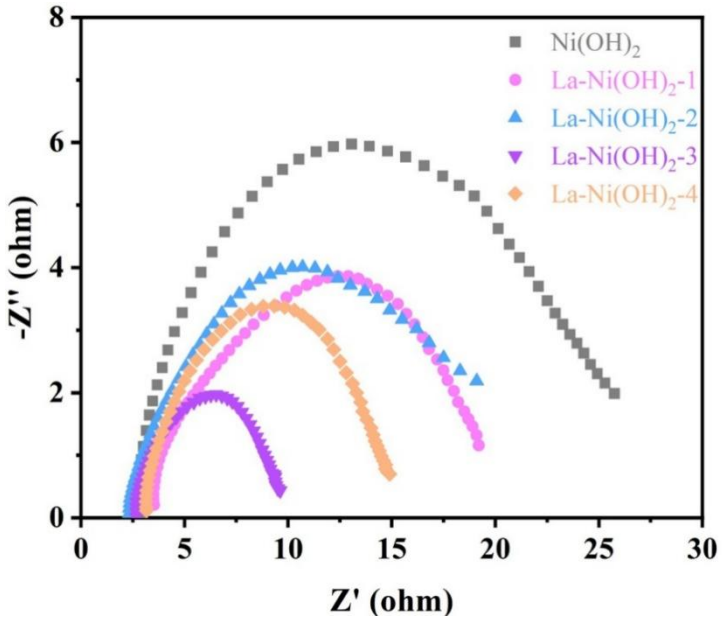

Figure S10. The electrochemical impedance spectroscopy (EIS) plot of $Ni(OH)_2$ and various La-$Ni(OH)_2$ electrocatalysts.

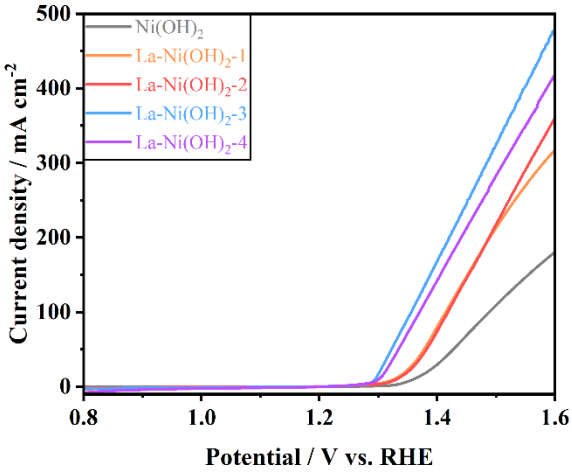

Figure S11. The iR-corrected LSV curves of $Ni(OH)_2$ and various La-$Ni(OH)_2$ electrocatalysts in 1 M KOH with 0.33 M urea solution.

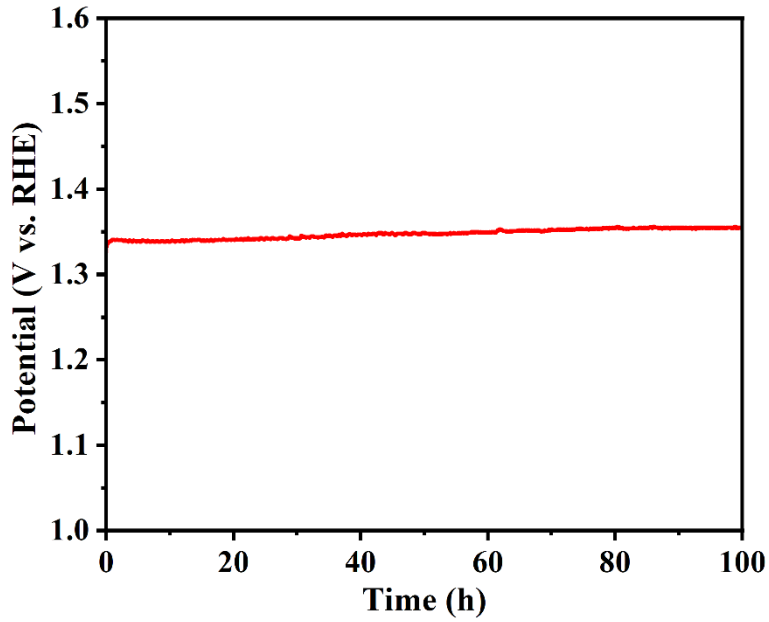

Figure S12. The chronopotentiometry curves stability for La-Ni$(OH)_2$-3 in 1 M KOH with 0.33 M urea solution.

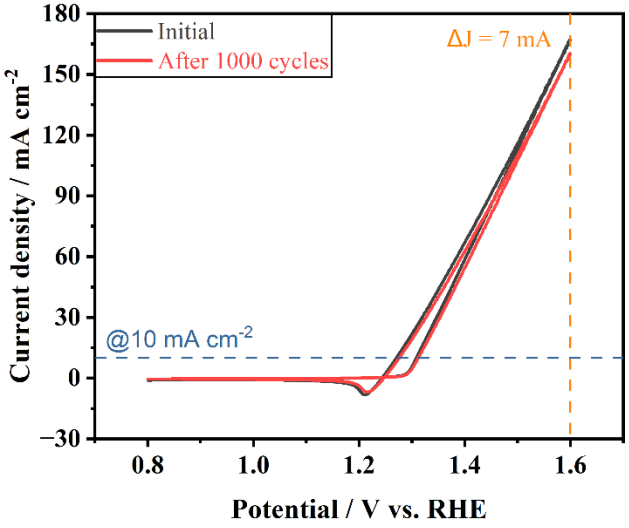

Figure S13. Comparison of CV curves before and after 100-hour stability test in 1 M KOH with 0.33 M urea solution.

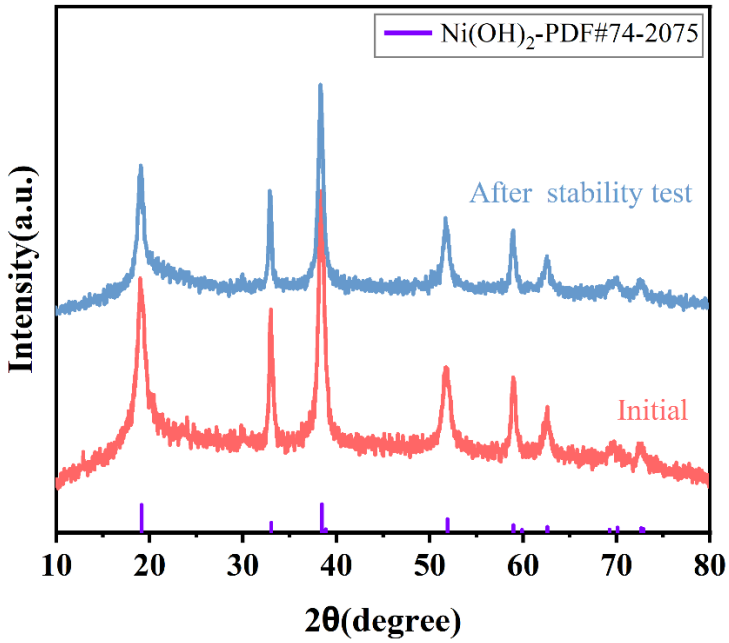

Figure S14. The XRD pattern of La-Ni(OH)$_2$ after the stability test.

Table S1. The corresponding amount of La present in each doped samples were estimated by an inductively coupled plasma optical emission spectrometer (ICP-OES).

Samples	La-Ni(OH)$_2$-1	La-Ni(OH)$_2$-2	La-Ni(OH)$_2$-3	La-Ni(OH)$_2$-4
La (wt%)	1.02	2.36	3.78	6.42

Table S2. Compare the UOR performance of La-$Ni(OH)_2$ with other reported UOR electrocatalysts.

catalyst	η@10 mA cm^{-2} (V vs. RHE)	j@1.6 V (mA cm^{-2})	Tafel slope (mV dec^{-1})	Stability (h)	Ref.
La-$Ni(OH)_2$-3	1.308	167	48.79	100	This work
$Ni(OH)_2$/CuCo/$Ni(OH)_2$	1.333	~112	92	50	[8]
Se–$Ni(OH)_2$	1.34	~117.8	67.4	100	[9]
$Ni(OH)_2$-Ni_3S_2/NF	1.346	~120	175.7	15	[10]
Cl_{32}–$Ni(OH)_2$	1.345	111.78	42.37	15	[11]
$Ni(OH)_2$/NiOOH	1.341	~160	26	50	[12]
WM-$Ni_{0.99}Co_{0.01}(OH)_2$	1.37	~52	31	24	[13]
$NiTe_2$/$Ni(OH)_2$/CFC	1.355	~65	-	30	[14]
MoO_3/V_2O_5/$Ni(OH)_2$	1.351	-	42	50	[15]

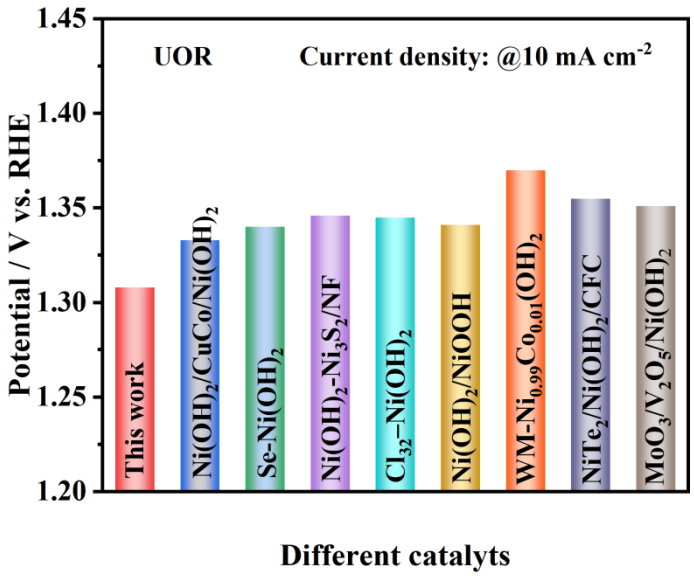

Figure S15. Compare the UOR current density at 10 mA cm^{-2} of La-$Ni(OH)_2$ with other reported UOR electrocatalysts.

S4. DFT calculations

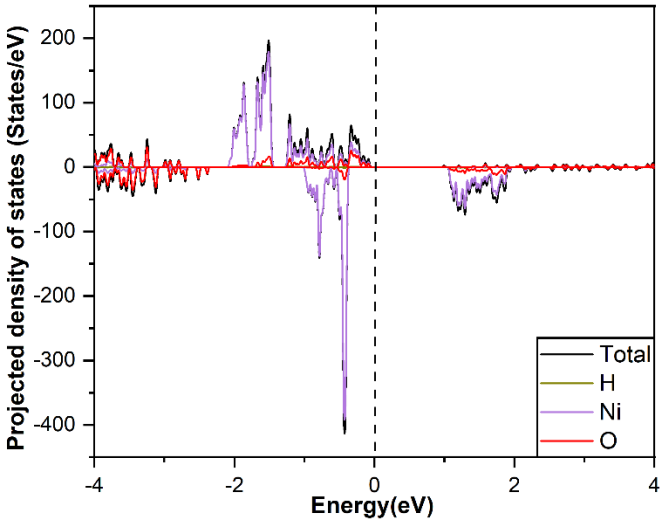

Figure S16. Projected density of states (PDOS) plots for $Ni(OH)_2$ surfaces.

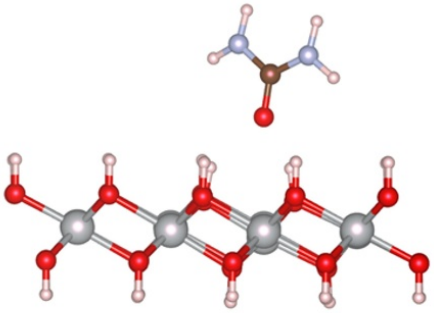

ΔE_{ad}= –0.36 eV

Figure S17. The optimized vertical adsorption configurations and energy of urea on $Ni(OH)_2$ surfaces. (Color code: Ni: gray, C: brown, O: red, N: cyan, H: pink).

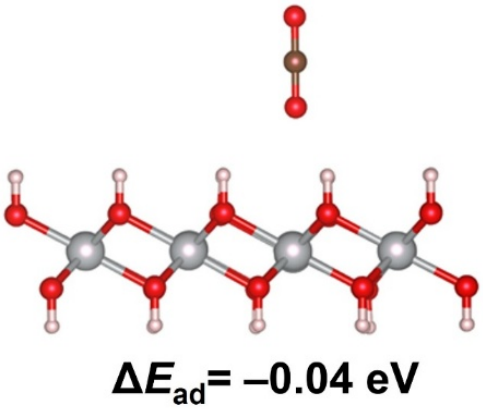

Figure S18. The optimized vertical adsorption configurations and energy of CO_2 on $Ni(OH)_2$ surfaces. (Color code: Ni: gray, C: brown, O: red, H: pink).

References

[1] Taylor, H. S.; Armstrong, E. F., A theory of the catalytic surface. *Proceedings of the Royal Society of London. Series A, Containing Papers of a Mathematical and Physical Character* **1925,** 108 (745), 105-111.

[2] Kresse, G.; Furthmüller, J., Efficient iterative schemes for ab initio total-energy calculations using a plane-wave basis set. *Physical Review B* **1996,** 54 (16), 11169-11186.

[3] Blöchl, P. E., Projector augmented-wave method. *Physical Review B* **1994,** 50 (24), 17953-17979.

[4] Kresse, G.; Joubert, D., From ultrasoft pseudopotentials to the projector augmented-wave method. *Physical Review B* **1999,** 59 (3), 1758-1775.

[5] Perdew, J. P.; Burke, K.; Ernzerhof, M., Generalized Gradient Approximation Made Simple. *Physical Review Letters* **1996,** 77 (18), 3865-3868.

[6] Grimme, S.; Antony, J.; Ehrlich, S.; Krieg, H., A consistent and accurate ab initio parametrization of density functional dispersion correction (DFT-D) for the 94 elements H-Pu. *The Journal of Chemical Physics* **2010,** 132 (15), 154104.

[7] Monkhorst, H. J.; Pack, J. D., Special points for Brillouin-zone integrations. *Physical Review B* **1976,** 13 (12), 5188-5192.

[8] Parvin, S., Aransiola, E., Ammar, M., Lee, S., Zhang, L., Weber, J.; Baltrusaitis, J., Tailored $Ni(OH)_2$/CuCo/$Ni(OH)_2$ composite interfaces for efficient and durable urea oxidation reaction. *ACS Applied Materials & Interfaces* **2024,** 16(49), 67715-67729.

[9] Song, S.; Huang, X.; Yang, Y.; Feng, L., Se self-doped Ni $(OH)_2$ for an efficient urea oxidation reaction. *Chemical Communications* **2024,** 60(78), 10906-10909.

[10] Zhou, L.; Feng, D.; Liu, C.; Sun, Y.; Fu, Y.; Ma, T., Amorphous $Ni(OH)_2$-Ni_3S_2/NF nano-flower heterostructure catalyst promotes efficient urea assisted overall water splitting. *Chemistry–An Asian Journal* **2024,** *19*(3), 202300980.

[11] Zhao, Y.; Sun, X.; Cao, Q.; Zhou, J.; Tan, W.; Piao, Z.; Liu, E.; Ding, R.; Gao, P.; Lin, W., Accelerating charge transfer for $Ni(OH)_2$ through chlorine-anion decoration in the urea electrooxidation reaction. *New Journal of Chemistry* **2023,** 47(19), 9483-9491.

[12] Long, G.; Chen, L.; Chen, X.; Liu, H.; Xiong, W.; Sun, X.; Hao, F., Interface engineering in $Ni(OH)_2$/NiOOH heterojunction to enhance energy-efficient hydrogen production via urea electrolysis. *Journal of Colloid and Interface Science* **2025,** *680*, 880-889.

[13] Liu, Y.; Yang, Z.; Zou, Y.; Wang, S.; He, J., Trace cobalt doing and defect engineering of high surface area α-$Ni(OH)_2$ for electrocatalytic urea oxidation. *Energy & Environmental Materials* **2024,** 7(2), 12576.

[14] Xu, B.; Yang, X.; Liu, X.; Song, W.; Sun, Y.; Liu, Q.; Yang, H.; Li, C., Lattice distortion in hybrid $NiTe_2$/$Ni(OH)_2$ nanosheets as efficient synergistic electrocatalyst for water and urea oxidation. *Journal of Power Sources* **2020,** 449, 227585.

[15] Zhang, Y.; Luo, K.; Peng, L.; Zhong, J.; Zhang, C.; Yuan, D., MoO_3/V_2O_5/$Ni(OH)_2$ with multiple heterojunction interfaces for the hydrogen preparation from urea-containing wastewater. *International Journal of Hydrogen Energy* **2025,** 107, 410-418.